Advances in Concrete Construction, *Vol. 2, No. 1 (2014) 57-75*
DOI: http://dx.doi.org/10.12989/acc.2014.2.1.057

Failure mechanisms of hybrid FRP-concrete beams with external filament-wound wrapping

A. Chakrabortty and A. Khennane*

School of Engineering and Information Technology, UNSW Canberra, Northcott Drive, Canberra , Australia

(Received February 10, 2014, Revised March 5, 2014, Accepted March 7, 2014)

Abstract. This paper presents an analysis of the results of an experimental program on the performance of a novel configuration of a hybrid FRP-concrete beam. The beam section consists of a GFRP pultruded profile, a CFRP laminate, and a concrete block all wrapped up using filament winding. It was found that the thickness of the concrete block and the confinement by the filament-wound wrapping had a profound effect on the energy dissipation behaviour of the beam. Using a shear punching model, and comparing the predicted results with the experimental ones, it was found that beyond a given value of the concrete block thickness, the deformational behaviour of the beam shifts from brittle to ductile. It was also found that the filament-wound wrap had many benefits such as providing a composite action between the concrete block and the GFRP box, improving the stiffness of the beam, and most importantly, enhancing the load carrying ability through induced confinement of the concrete.

Keywords: high strength concrete;steel fibers; finite element analysis (FEA); hybrid beam; pultrusion; filament winding

1. Introduction

At present, the only niche market for composite materials in highway bridges is in FRP (Fibre Reinforced Polymers) deck construction over steel girders. Fig. 1 from Harries (2008) shows the various applications of FRP materials within the Innovative Bridge Research and Construction (IBRC) Program conducted by the United States Federal Highway Administration. About one quarter of the bridges involve the use FRP decks as replacement for existing bridge decks on steel girders, and the number of all-FRP structures is insignificant. For an all FRP bridge, pultruded or hand layup GFRP profiles are the most indicated structural elements for use as girders. However, their lack of stiffness is a serious drawback given that bridge design is generally stiffness driven. Consequently, they results in very thick cross sections such as the ones used in the Tech21 Bridge (Farhey 2005), Fig. 2, or in a large number of girders, 24 as used in the two lane Tom's Creek Road Bridge (Neely 2004) shown in Fig. 3.

The alternative is to use hybrid girders hybrid FRP-concrete systems. They offer the benefits of combining the mass of concrete with the tailorable properties of FRP's. Such concepts have already been trailed by Deskovic *et al*. (1995), Canning *et al*. (1999), Zhao *et al*. (2000), van Erp

---

*Corresponding author, Professor, E-mail: a.khennane@adfa.edu.au

http://www.techno-press.org/?journal=acc&subpage=7 ISSN:2287-5301(Print)2287-531X(Online)

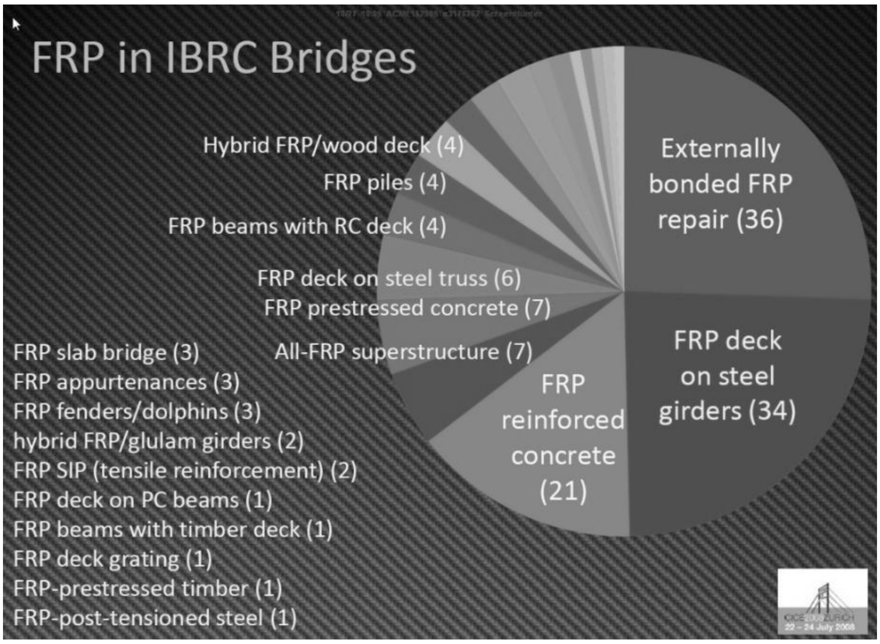

Fig. 1 Composites in bridges (Harries 2008)

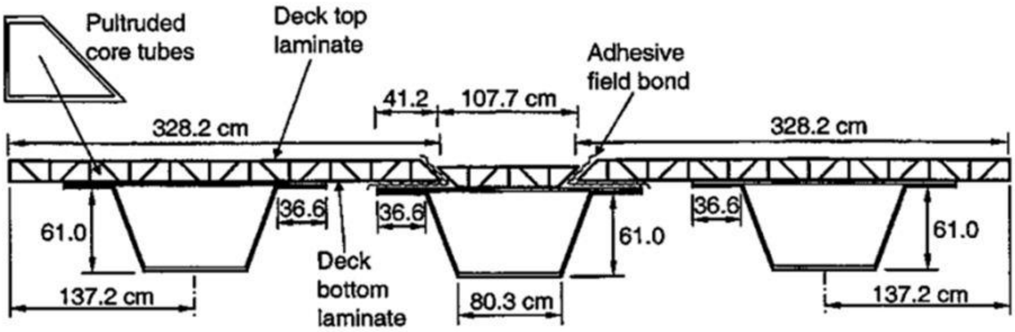

Fig. 2 Cross section of the tech21all composite bridge (Farhey 2005)

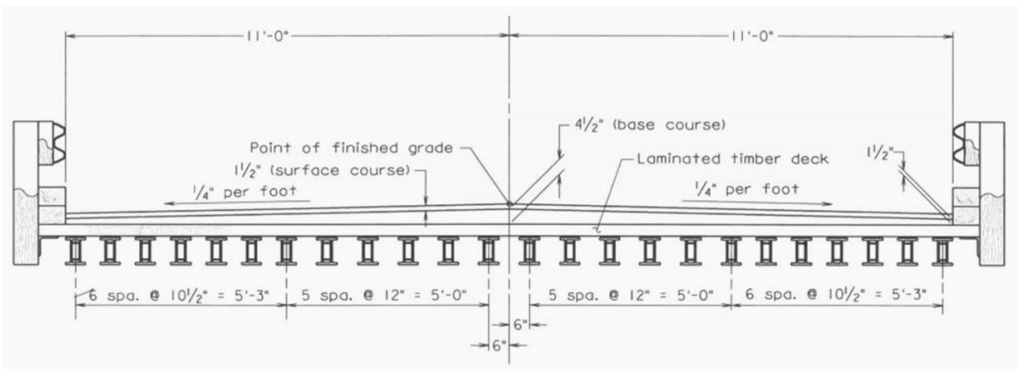

Fig. 3 Cross section of Tom’s creek road bridge (Neely *et al*. 2004), (1"= 25.4 mm)

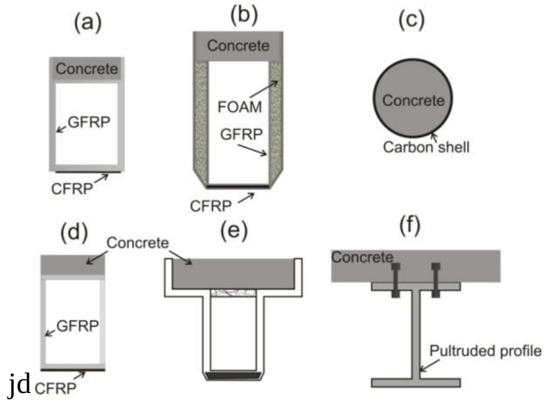

Fig. 4 Existing hybrid FRP-concrete beam designs

et al. (2005), Hulat *et al*. (2003), and Correia *et al*. (2007). Their respective cross section designs are shown on Fig 4. Deskovic *et al*. (1995) Fig. 4(a), Canning *et al*. (1999) Fig. 4(b), and van Erp *et al*. (2005) Fig. 4(d), use almost similar designs, where the beams consist of a custom made FRP box, a concrete layer, and a CFRP laminate to serve as a warning of imminent collapse. Yet, this approach simply mimics that of reinforced concrete in the sense that the CFRP failure is expected to replace steel yielding. As a result, the CFRP laminate is usually very thin, and contributes very little to the stiffness of the beam. Having recognized the inherent lack of stiffness of GFRPs, Zhao *et al*. (2000) opted for a CFRP shell filled with concrete as shown on Fig. 4(c). The carbon shell has both hoop reinforcement (90^o from longitudinal axis) and $\pm\ 10^o$ longitudinal fibers, as well as helical ribs on the inside to ensure full force transfer with the concrete. This design resulted in a stiff girder, but the load versus displacement curves obtained under four point bending were linear up to failure, and did not exhibit any signs of imminent failure. Correia *et al*. (2007) tested a hybrid beam which consisted of a pultruded section and a concrete layer. A preliminary test proved that the adhesion between the pultruded profile and the concrete was insignificant. As a result, the shear connection in subsequent beams had to be provided using mechanical means as shown in Fig. 4(f). The beams failed without warning due to shear in the GFRP profile, which occurred in the top flange junction. In summary, the short comings of the previously described designs can be listed as follows:

• custom made GFRP boxes or carbon shell have a high initial cost;

• being very thin to serve a warning for imminent failure, the CFRP laminate contributes very little to the overall stiffness of the beam;

• when a cost effective pultruded profile is used, mechanical means are needed to provide the shear connection with the concrete

2. New design

To address the previously described shortcomings of hybrid beams, Khennane (2009) and Chakrabortty *et al*. (2011) have taken this idea a stage further with the rectangular section member manufactured from pultruded GFRP composite and a CFRP laminate in the tension zone. The whole system including the concrete in the compression zone is confined with a wrapping

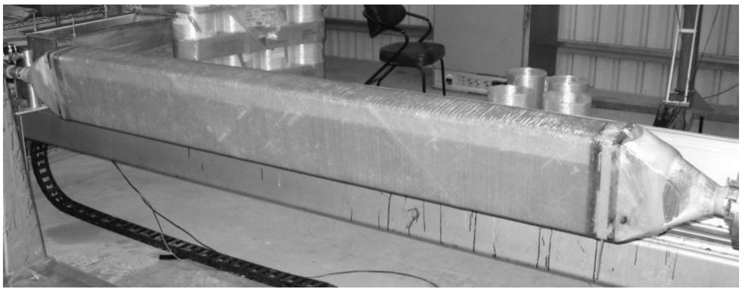

Fig. 5 Externally filament wound hybrid beam

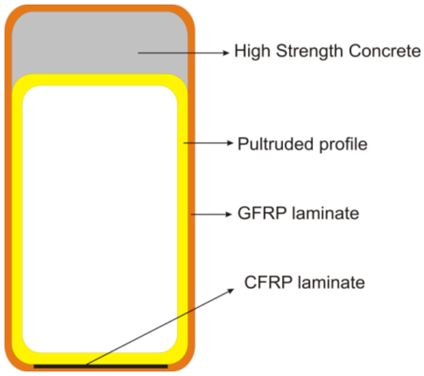

Fig. 6 Proposed design for a hybrid FRP-Concrete beam

Fig. 7 NSC and SFHSC series of beams with different concrete blocks'thicknesses

consisting of external filament winding to ensure composite action between the GFRP box and the concrete block. Fig. 5 shows a photograph of the beam and Fig. 6 a schematic representation of its cross section. It is also worth mentioning that the idea of using filament winding as a wrapping is not new. It was first used by Parsons *et al*. (2002) to develop a bridge superstructure, which consisted of two components: a series of inner cells, lying parallel to the direction of traffic, and an outer filament wound shell. Williams *et al*. (2003) also developed three generations of hybrid FRP concrete decks using pultrusion and filament-winding techniques. Feng *et al*. (2006) used filament winding to wrap GFRP pultruded profiles for use as bridge decking. It was found that the outside filament wound reinforcement enhanced the load carrying ability of the profiles.

To minimize the cost of the beam, a pultruded GFRP box profile, available "off the shelf", is chosen. Thin walled box sections are very efficient for beams, and they have a high resistance to lateral torsional buckling. To address the inherent lack of stiffness of hybrid beams, the CFRP laminate is not designed to fail first to give a warning of imminent failure; the details of the design are reported in Chakrabortty *et al*. (2011). Instead, its primary role is to provide the required stiffness for the beam. As such, there is no upper limit on its thickness. Therefore, the stiffness of the beam can be tailored. The warning of imminent failure is hoped to be achieved through the crushing of the concrete. The addition of the filament wound outer laminate serves two purposes. Its principal role is to provide some form of confinement to the system concrete block-pultruded profile as to ensure a composite action, thus eliminating the risk of debonding failure. The lack of composite action between the concrete and the laminates was reported as a serious shortcoming of these sections (Canning *et al*. 1999, Correia *et al*. 2007). Finally, with fibers oriented at $\pm 45^o$, its second role is to improve the shear strength of the pultruded profile, which has fibers predominantly in the longitudinal direction.

The detailed experimental program is reported in Chakrabortty *et al.* (2011). In total six beams as shown in Fig. 7 were tested; three with Normal Strength Concrete (NSC) blocks, and three with Steel Fibers reinforced High Strength Concrete (SFHSC) blocks. The mechanical properties of the materials are given in Tables 1 and 2.

Table 1 Mechanical properties of concrete

Concrete Type	Elastic modulus (MPa)	Compressive strength (MPa)	Ultimate compressive strain
NSC	23140	38.83	0.0032
SFHSC	33330	88.20	0.0034

Table 2 Mechanical properties of the pultruded profiles

Pultruded profile cross section	Longitudinal modulus, E_L (MPa)	Transverse modulus, E_T (MPa)	Shear modulus G_{LT} (MPa)
200 × 100 × 10	28870	3510	2980

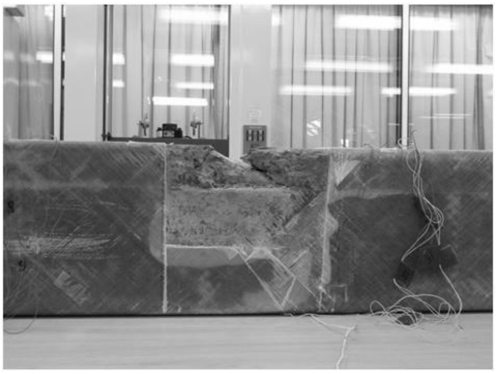

Fig. 8 Punching shear failure of the concrete block

3. Proposed novel approach

It was noticed that when the concrete block is thin, the beams failed prematurely through shear punching of the concrete block as shown in Fig. 8. Adapting the method originally developed by Yankelevski and Leibowitz (1999) for predicting the ultimate shear punching capacity of reinforced concrete slabs, it is possible to estimate the shear punching capacity of the concrete block. The proposed model considers the final failure stage of the concrete block as schematically shown in Fig. 10. It is assumed that the system's resistance is concentrated along the failure surfaces.

Like in the original model of Yankelevski and Leibowitz (1999)**,** the following assumptions need to be made:

- concrete is ideally rigid and the cracked surfaces subdivide the concrete block into three parts;
- the deformation and the accompanied resistance are concentrated along the cracked surfaces;
- the cracked failure surfaces are rough and a mechanism of aggregate interlock is developed; and
- the contribution of the pultruded profile is neglected.

The loading platen pushes the punched concrete wedge through the block. The relative displacement u between the two rigid bodies, as shown in Fig. 10, can be resolved into two displacement components: a tangential displacement component, Δ and a normal displacement, . The first component increases the crack width and the second component produces shear. The rough crack surface geometry is responsible for dilation or crack opening. When the dilation is restrained, compressive stresses are developed normal to the crack.

Variations in the shear and the normal stresses acting on the cracked surface are functions of the crack displacement. They can be expressed as follows:

$$\tau = A \times \Delta + B \tag{1}$$

$$\sigma = X \times \Delta + Y \tag{2}$$

where the parameters A, B, X and Y are functions of the shear displacement Δ and the crack width w. They can be obtained from the data (Walraven 1981) shown in Fig. 11. The linear relationships have been chosen for reasons of simplicity, otherwise the original nonlinear relationship (Walraven 1981) could be adopted. Note that the data presented on Fig. 11 were obtained for a concrete strength of 59.1 MPa, while the normal concrete used in the present beams has only a strength of 38.8 MPa. However, as will be shown in the subsequent section, it is believed that the strength of the concrete is enhanced to some extent due to the confinement introduced by the filament-wound wrapping. It is assumed therefore that the use of these data in the present case is warranted.

The shear displacement, Δ, and crack width, w, for the punched wedge can be expressed as

$$\Delta = u \cos\alpha \tag{3}$$

$$w = u \sin\alpha \quad \text{with} \quad \alpha = 90^o - \theta \tag{4}$$

Fig. 9 Concrete crushing in beam SFHSC_B3

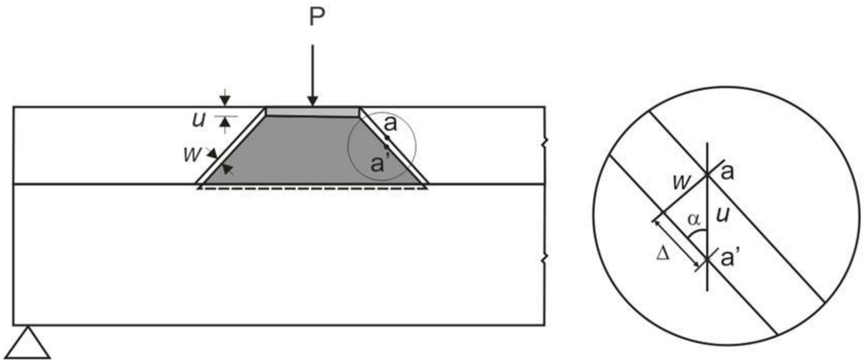

Fig. 10 Schematic diagram of punching shear failure of the concrete block

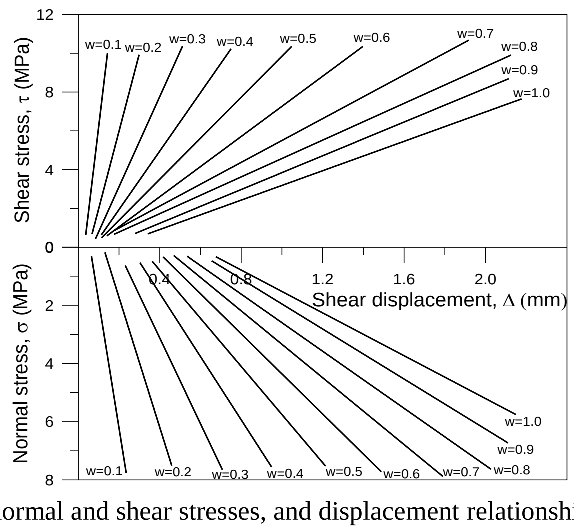

Fig. 11 Simplified normal and shear stresses, and displacement relationships (Walraven 1981)

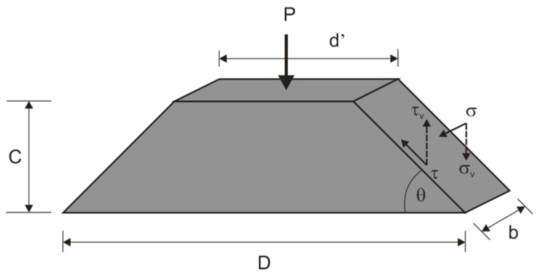

Fig. 12 Punched wedge of the concrete block

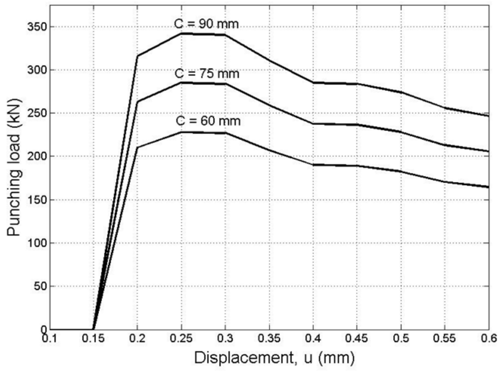

Fig. 13 Punching load-displacement relationship

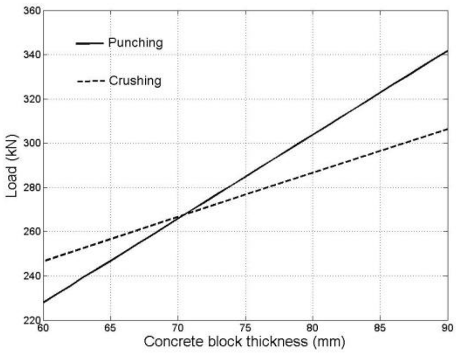

Fig. 14 Punching and crushing loads as a function of C/H of a span of 2 meters

When the concrete wedge is isolated as a free body diagram as shown on Fig. 12, the force components distributed along the surfaces of the cracks can be integrated to yield the magnitude of the forces. Note that *c* represents the thickness of the concrete block, d' the loading plate width, *D* the length of the bottom of the wedge, *u* the width of the concrete block and θ the crack angle.

The total surface of the cracked area is obtained as

$$S = 2 \times b \times C / \sin\theta \tag{5}$$

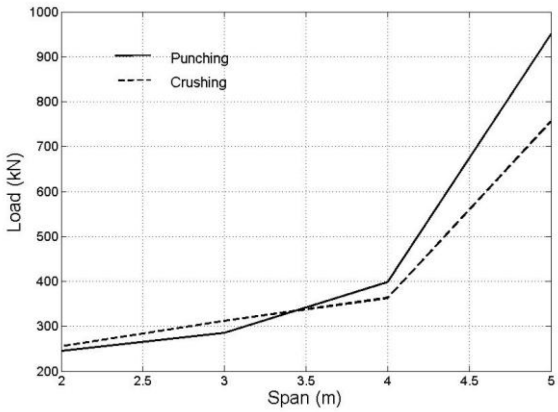

Fig. 15 Punching and crushing loads as a function of the span for a C/H = 0.25

Multiplying the total area of the cracks by the vertical shear stress component, yields the tangential shear force as

$$P_{\tau v} = S\tau \sin\theta \tag{6}$$

Similarly, the vertical component of the normal stress can be obtained as

$$P = P_{\tau v} - P_{\sigma v} \tag{7}$$

Considering an angle of 58°, which was estimated from the dimensions of the punched wedge, and varying the displacement *u* from 0 onwards, it is possible to plot the punching load *P* as a function of the displacement *u*. For every value of *u*, Δ and *w* can be obtained from equations (3) and (4). Using these values, the tangential and normal stresses can be read or interpolated from Fig. 11. These are then substituted in equations (1), (2), (6) and (7) to obtain the punching force *P*.

Fig. 13 shows the computed punching load displacement curves for the beams NSC_B1, NSC_B2 and NSC_B3 which have different concrete block thicknesses. As expected, the thicker the concrete block, the bigger is the force required to punch through it. The punching load first increases to reach a maximum before it drops in a fashion similar to the observed softening behavior of concrete.

The punching failure loads obtained from equation (7) for these three beams are also presented in Table 3 and compared with the experimental failure loads and the predicted failure loads using strain compatibility as detailed in Chakrabortty *et al*. (2011). It can be seen that the predicted punching load for beam NSC_B1 is less than the load predicted from its crushing strain, which is in agreement with its premature failure through shear punching. However, for the other two beams the predicted punching load are higher than the loads calculated using strain compatibility and concrete crushing strain. These predictions are also in line with the recorded experimental results. Indeed, both beams failed through crushing of the concrete block.

Similar observations were also noted for the steel fiber reinforced high strength concrete (SFHSC) beams. The beam SFHSC_B1 with a concrete block thickness of 60 mm also failed prematurely due to punching shear. Unfortunately, the model presented here can only predict the

Table 3 Experimental and predicted loads comparison of NSC beams

Beam	C in mm	C/H	Predicted flexure load kN	Punching kN	Test load kN	Failure type
NSC_B1	60	0.23	246.57	227.84	214.40	Shear punching
NSC_B2	75	0.27	276.74	284.81	279.80	Concrete crushing
NSC_B3	90	0.31	306.35	341.77	332.10	Concrete crushing

Table 4 Experimental and predicted loads comparison of SFHSC beams

Beam	C mm	C/H	Predicted flexure load kN	Test load kN	Failure type
SFHSC_B1	60	0.23	334.87	361.30	Punching shear
SFHSC_B2	75	0.27	376.12	371.00	Concrete crushing
SFHSC_B3	90	0.31	414.38	416.00	Concrete crushing

punching failure loads for beams with a maximum concrete strength of 59.1 MPa, and the strength of the SFHSC in unconfined condition is measured to be 88.2 MPa. In addition, the assumptions in the developed model are based on normal strength concrete, which are not applicable to SFHSC due to the existence of fibers. Due to the unavailability of test data for the SFHSC, it is not possible therefore to calculate the normal and shear stresses developed on the cracked surface of the SFHSC block. As a result, only the experimental failure loads and those predicted using strain compatibility are shown in Table 4.

It is very clear that the thickness of the concrete block governs the behavior of the beam. It is therefore of paramount importance to estimate the ratio of the concrete block to that of the section, C/H, at which the failure shifts from shear punching to the desired concrete crushing. However, this can be done for beams with a normal concrete block since the developed shear punching model is only applicable to this material. For a constant span of 2 meters and a constant height H = 200 mm of the pultruded profile, varying the concrete block thickness from 60 to 90 mm, and using the present shear punching model and the strain compatibility model developed in Chakrabortty *et al.* (2011), it is possible to plot the shear punching load and the concrete crushing loads as a function of C/H. Fig. 14 shows a plot of the predicted shear punching failure load and the flexural failure load predicted using strain compatibility. It can be seen that the failure shifts from shear punching to concrete crushing at a ratio of C/H between 0.23 and 0.27. The preceding results however are only valid for the section and the span tested.

By choosing the height of the section as a parameter H = L/10, where L represents the span, and fixing the height of the concrete block as C = H/4, it is possible to plot the shear punching and the crushing loads as a function of the span. The results are shown on Fig. 15. It can be seen that for a span in excess of 3.5m, as is the case for most bridges, crushing of the concrete becomes the predominant failure mode, and the ratio of C/H = 0.25 is more than adequate.

In summary, it can be said that the concrete block thickness significantly controls the overall beams' behavior. A relatively lower thickness of the concrete block would result in premature failure of the beam through punching shear, and would not allow it to perform to its full capacity. In order to achieve the best performance from the concrete block, a relationship between the concrete block thickness and the section height is presented. It was found that a concrete block thickness of 25 % of the section is enough for spans in excess of 3.5 m to result in the crushing of the concrete controlling the failure of the beam.

4. Confinement

4.1 Stress strain curve of partially confined concrete

In the present case the concrete block is confined on three sides by the filament-wound wrapping and on the fourth side by the pultruded profile. The experimental results revealed that there is a confinement effect on the concrete. What is not clear, however, is the extent of this confinement. The tests were carried under four point bending. In the region of maximum bending moment, the concrete can be considered under a state of uni-axial compression, albeit non-uniform, hence the assumption of a partial confinement. Using finite element analysis, this effect is investigated in the following sections.

According to Lam and Teng (2003) and Csuka and Kollar (2010), confined concrete displays different stress-strain curves according to the amount of confinement as shown in Fig. 16. When the concrete is fully confined the stress-strain curve shows a monotonically ascending bilinear shape; i.e., increasing type (Fig. 16(b)), which is the general case for a circular confinement as has been reported by many researchers (Lam and Teng 2003[a], Csuka and Kollar 2010, Fam and Rizkalla 2001, Samman *et al*. 1998 and Xiao and Wu 2003). For fully confined circular sections, the FRP-confinement is able to play its role completely and provides variable confining pressures on the concrete as it maintains an appreciable amount of stiffness throughout the loading process, and ultimately fails by rupture.

Experimental evidence has also shown that such a bilinear stress-strain response cannot always be obtained, and the peak stress is reached before the rupture of FRP wrapping; i.e., a descending type (Lam and Teng 2003[b]). Moreover, there are two types of descending branches. In the first case, when the concrete is sufficiently confined, the axial stress at ultimate strain is higher than the unconfined concrete strength, Fig. 16(c), and there will be a significant improvement in the strength due to confinement. In the second case, the ultimate axial stress is less than the peak unconfined concrete strength; Fig. 16(d), and there will be a little enhancement in the concrete strength due to the confinement. Such a concrete is insufficiently confined, and this behavior is more pronounced for rectangular sections.

The concrete section in the present beams is also rectangular, and can be therefore considered as partially confined. Most importantly, the concrete in the beam crushed before FRP rupture, which is consistent with insufficient confinement as reported by Xiao and Wu (2003) and Aire *et al*. (2001). It follows therefore that in the present case, it can be reasonably assumed that the stress-strain curve shown in Fig. 16(d) would be the most suitable one for this analysis. Unfortunately, there are no available models that could predict the stress-strain behavior of this type of partially confined rectangular concrete sections. As a result, it was necessary therefore to develop a partially confined concrete material model to produce a stress strain curve that can be used in the subsequent finite element analysis.

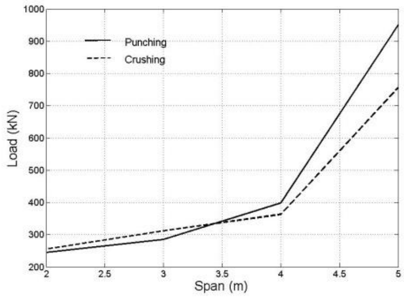

Fig. 15 Punching and crushing loads as a function of the span for a C/H = 0.25

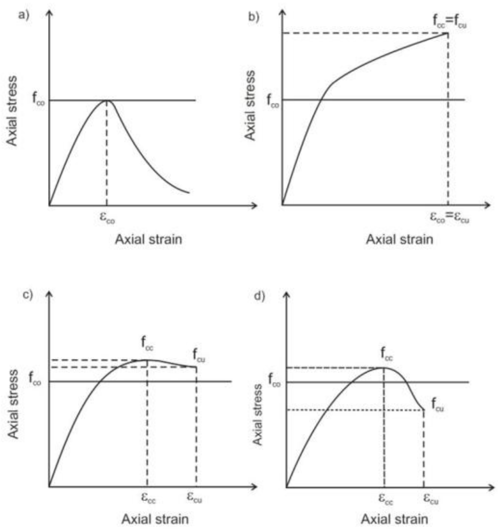

Fig. 16 Stress-strain curves for confined concrete

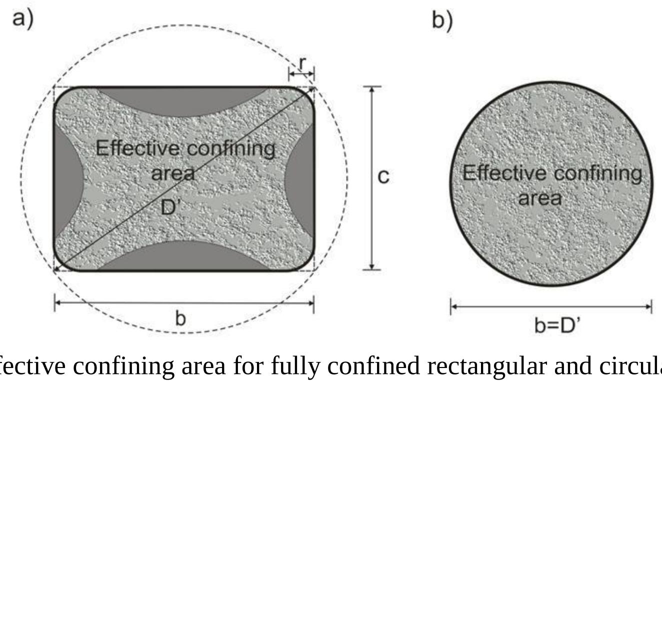

Fig. 17 Effective confining area for fully confined rectangular and circular sections

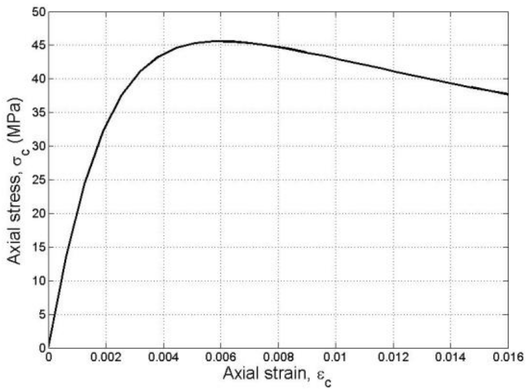

Fig. 18 Compressive stress-strain curve for partially confined concrete

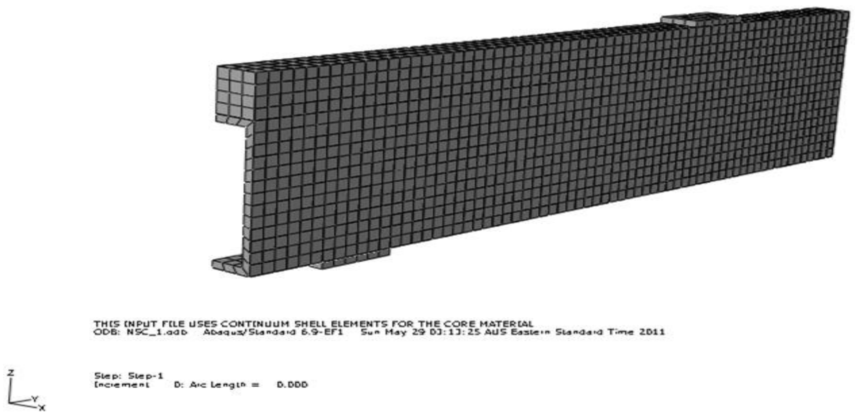

Fig. 19 Finite element model

Most of the FRP-confined concrete models available for evaluating the amount of increase in the concrete strength and corresponding peak axial strain are based on the confined concrete model developed experimentally by Richart *et al*. (1928, 1929) which is given by

$$\frac{f_{cc}}{f_{co}} = 1 + k_1\left(\frac{f_l}{f_{co}}\right) \tag{8}$$

$$\frac{\varepsilon_{cc}}{\varepsilon_{co}} = 1 + k_2\left(\frac{f_l}{f_{co}}\right) \tag{9}$$

where, f_{cc} and ε_{cc} represent the peak axial stress and corresponding strain of the confined concrete, f_1 the confining pressure, k_1 the confinement effective coefficient, and $k_2 = k_1$.

Based on the test results for concrete cylinders actively confined by spiral steel stirrups, Richart *et al*. (1928) proposed a value of 4.1 for k_1. The parameter k_1 is a function of the confinement level and of the concrete strength, for which a wide range of other values of k_1 have also been proposed both experimentally and analytically (Samman *et al*. 1998, Toutanji *et al*. 2010, Mirmiran and Shahawy 1997, Shehata *et al*. 2002). However, the values available in the literature are not suitable for the present case as the concrete block is rectangular and partially confined. Therefore, it was decided to choose the value of k_1 for this analysis based on a trial and error basis.

The confining pressure, f_1, supplied by the filament-wound wrapping on the concrete of the beam is required in Eq. (8). It is obtained as

$$f_l = \frac{2E_{frp} t \varepsilon_{frp}}{D'} k_s \tag{10}$$

where, E_{frp} is the elastic modulus of the wrapping in the hoop direction; ε_{frp} the tensile rupture strain of the wrapping; t the thickness of the wrapping; and D' the diameter of the circular section. However for square or rectangular section, D' is considered as the diagonal length of that section (Lam and Teng 2003[b] , Al-Salloum 2007) as shown in Fig. 17(a).

In Eq. (10), k_s is the shape factor that depends on the effective confining area of the cross-section. It is and commonly used for both rectangular and square sections. The effective confining area for a rectangular section is the area contained by four parabolas (Fig. 17(a)). Therefore, for a fully confined rectangular section k_s is defined as the ratio of the effective confined area to the total area of the cross-section. Limiting the expression presented by Lam *et al*. (2003[b]) to a rectangular section with round corners and of plain concrete, k_s can be expressed as

$$k_s = 1 - \frac{\frac{b}{c}(b-2r)^2 + \frac{c}{b}(c-2r)^2}{3\left\{bc - (4-\pi)r^2\right\}} \tag{11}$$

However, the concrete section in the beam is rectangular and partially confined; therefore, the effective confining area will be less than what is shown in Fig. 17(a). Since the exact amount of effectively confined area for this partially confined concrete section is unknown, the minimum value of the shape factor as suggested by Pessiki *et al*. (2001) will be therefore chosen for this analysis.

The stress strain curve required for this analysis is generated from the complete stress-strain relationship given by Teng *et al*. (2007) as

$$\sigma_c = f_{cc}\left\{\frac{(\varepsilon_c/\varepsilon_{cc})r}{r-1+(\varepsilon_c/\varepsilon_{cc})^r}\right\} \tag{12}$$

where ε_c is the axial strain of concrete, f_{cc} and ε_{cc} the peak axial stress and corresponding strain of confined concrete which are given in Eqs. (8) and (9), r a constant used to account the brittleness of concrete (Carriera and Chu 1985) as

$$r = \frac{E_c}{E_c - f_{cc}/\varepsilon_{cc}} \tag{13}$$

From this partially confined concrete model several stress-strain curves can be generated for different values of k_1. Fig. 18 shows a typical curve obtained with k_1 = 1.5, deemed suitable for this analysis, which yields a corresponding value of k_2 equal to 7.5. Due to partial confinement, there is a strength enhancement of about 20 % as shown in Fig. 18. Most importantly, the new stress strain curve shows a more ductile behavior.

4.2 Stress strain curve of partially confined concrete

To investigate the extent of the confinement introduced by the filament winding wrap, the general purpose finite element software ABAQUS (2009) is used. Due to symmetry, only one quarter of the beam is modeled as shown in Fig. 19.

The concrete block is meshed with solid 8-noded continuum three dimensional brick elements, the pultruded profile is meshed with 8-noded continuum shell elements and, due to relatively smaller thicknesses, both the CFRP and the outer GFRP filament-wound wrapping are meshed with 4-noded conventional shell elements. The support and loading plates are also meshed using the 8-noded continuum three dimensional brick element. The concrete damage plasticity model (CDPM) is used for concrete, while the FRP model including damage initiation and evolution also provided in ABAQUS is used for the composite components.

Two beams NSC_B2 and NCS_B3, made of normal concrete with a cylinder strength of 38.83 MPa and having different concrete block thicknesses, respectively equal to 75 mm and 90 mm, are analyzed. Fig. 20 and 21 show the obtained results. It can be seen that when the stress-strain curve of the concrete is used as is; that is without the effect of confinement, the predicted ultimate load carrying abilities of the beams are less than the recorded experimental ones. On the other hand, when the confined stress-strain curve is used, the finite element result predicted the concrete crushing and failure loads reasonably well. This indicates that the wrapping does indeed confine the concrete block, and hence provides some extra load carrying ability.

Similarly, the beams with a steel fibre reinforced concrete block that did not fail through shear punching were analyzed using ABAQUS. This analysis however required a separate concrete material model to account for the steel fibers. Use is made therefore of the stress stress-strain relationship proposed by Mansur *et al*. (1999) for steel fiber reinforced high strength concrete defined as

$$\sigma_c = f'_{co}\left\{\frac{\alpha_1\beta\left(\dfrac{\varepsilon_c}{\varepsilon_o}\right)}{k_1\beta-1+\left(\dfrac{\varepsilon_c}{\varepsilon_o}\right)^{\alpha_2\beta}}\right\} \tag{13-a}$$

with

$$\alpha_1 = \left(\frac{50}{f'_{co}}\right)^3\left\{1+2.5\left(V_f A_R\right)^{2.5}\right\} \tag{13-b}$$

and

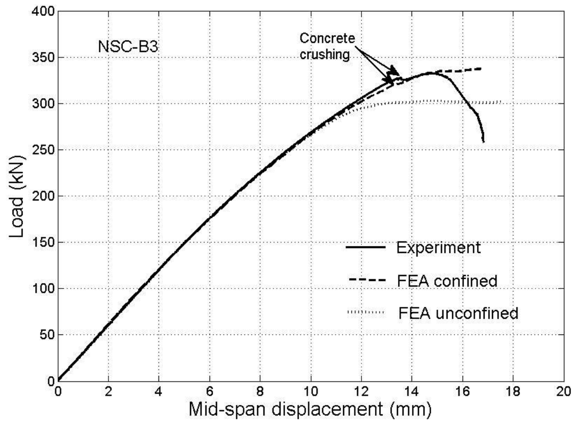

Fig. 21 Comparison of FEA and experimental response of the NSC_B3

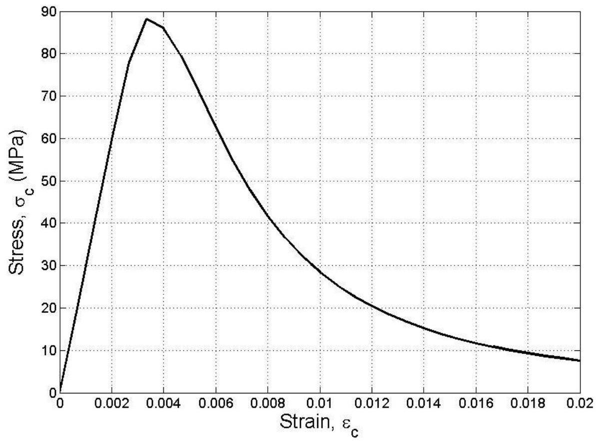

Fig. 22 Compressive stress-strain curve for SFHSC

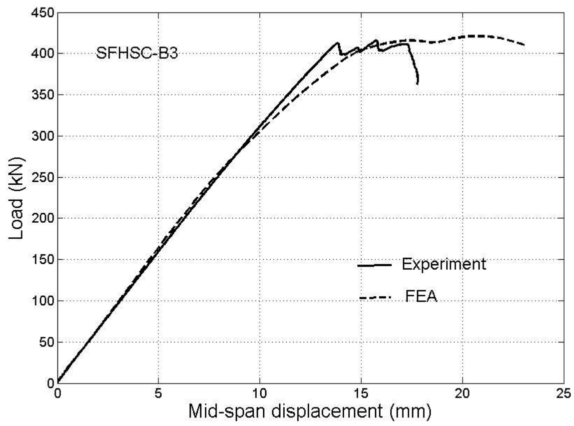

Fig. 23 Experimental and predicted load-displacement curves for SFHSC_B3

$$\alpha_2 = \left(\frac{50}{f'_{co}}\right)^{1.3} \left\{1 - 0.11\left(V_f A_R\right)^{-1.1}\right\} \tag{13-c}$$

The parameters a_1 and a_2 are constants that reflect the effect of the fibers; V_f is the fibre volume fraction; A_R is the fiber aspect ratio; and *ß* is a material parameter that depends on the shape of the stress-strain diagram, and is given by

$$\beta = \frac{1}{1 - \left(\frac{f'_{co}}{\varepsilon_o E_{it}}\right)} \tag{13-d}$$

where E_{it} is the initial tangent modulus given by

$$E_{it} = \left(10300 - 400V_f\right) f'^{\,1/3}_{co} \tag{13-e}$$

and ε_0 the strain at peak stress, also given as

$$\varepsilon_o = \left[0.0005 + 0.00000072\left(V_f A_R\right)\right]\left(f'_{co}\right)^{0.35} \tag{13-e}$$

where f'_{co} is the SFHSC compressive strength.

The stress-strain curve obtained from the above relations is shown on Fig. 22. Fig. 23 shows the predicted and experimental load-displacement curve for the beam SFHSC_B3. Note that the predicted curve is obtained without taking into account the effect of confinement. It can be seen that it agrees very well with the experimental one. The finite element result also predicted the concrete crushing and failure loads reasonably well. This indicates that the external wrapping did not have any effect of the steel fiber reinforced concrete. This does not come as a surprise since it has already been reported by many researchers that confinement is less effective for HSC than NSC (Ahmad and Shah 1983, Setunge *et al*. 2010). Although the confinement did not improve the concrete strength in this case, it did contribute to the overall performance of the beam as it kept the concrete block in its position and eliminated the debonding of concrete from the pultruded profile.

5. Conclusions

The results of an analysis of the data from an experimental program on the performance of a novel configuration of a hybrid FRP-concrete beams have revealed that the thickness of the concrete block and the confinement induced by the filament-wound wrapping had a profound effect on the energy dissipation behavior of the beams.

Using a shear punching model, it was found that beyond a given value of the concrete block thickness, the deformational behavior of the beam shifts from brittle to ductile. It was also found that a concrete block thickness of 25 % of the section is enough for spans in excess of 3.5 m to inhibit shear punching failure but also results in the crushing of the concrete controlling the failure of the beam.

The filament-wound wrap was found to have many benefits such as providing a composite action between the concrete block and the GFRP box, improving the stiffness of the beam, and, most importantly, enhancing the load carrying ability as well as its deformational properties through induced confinement of the concrete. This last point is particularly important to the construction industry, where design is mainly stiffness driven, and ductility is of paramount importance.

References

ABAQUS (2009), "Abaqus documentation", Version 6.9: *http://www.simulia.com*.

Ahmad, S.H. and Shah, S.P. (1983), "Stress-strain curves of concrete confined by spiral reinforcement", *ACI J.*, **79**(46), 484-490.

Aire, C., Gettu, R. and Casas, J.R. (2001), "Study of the compressive behavior of concrete confined by fiber reinforced composites", *Proceeding of the International Conference on Composites in Constructions*, Balkema, Lisse, The Netherlands, 239-243.

Al-Salloum, Y.A. (2007), "Influence of edge sharpness on the strength of square concrete columns confined with FRP composite laminates", *Compos. Part B: Eng.*, **38**, 640-650.

Canning, L., Hollaway, L. and Thorne, A.M. (1999), "Manufacture, testing and numerical analysis of an innovative polymer composite/concrete structural unit", *Proceedings – Institution of Civil Engineers, Struct. Build.*, **134**, 231-241.

Carreira, D.J. and Chu, K.H. (1985), "Stress-strain relationship for plain concrete in compression", *ACI J.*, **82**(6), 797–804.

Chakrabortty, A., Khennane, A., Kayali, O. and Morozov, E. (2011), "Performance of outside filament-wound hybrid FRP-concrete beams", *Compos. Part B: Eng.*, **42**(4), 907-915.

Correia, J.R., Branco, F.A. and Ferreira, J.G. (2007), "Flexural behaviour of GFRP-concrete hybrid beams with interconnection slip", *Compos. Struct.*, **77**, 66-78.

Csuka, B. and Kollar, L.P. (2010), "FRP-confined circular concrete columns subjected to concentric loading". *J. Reinf. Plast. Comp.*, **29**(23), 3504-3520.

Deskovic, N., Triantafillou, T.C. and Meier, U. (1995), "Innovative design of FRP combined with concrete: short term behaviour". *ASCE J. Struct. Eng.*, **121**(7), 1069-1078.

Fam, A.Z. and Rizkalla, S.H. (2001), "Confinement model for axially loaded concrete confined by circular fiber-reinforced polymer tubes", *ACI Struct. J.*, **98**(4), 451-461.

Farhey, N. (2005), "Long-term performance monitoring of the tech 21 all-composite bridge", *ASCE J. Compos. Construct.*, **9**(3), 255-262

Feng, P., Ye, L., Li, T. and Ma, Q. (2006), "Outside Filament-wound Reinforcement: A Novel Configuration for FRP Bridge Decks", *The Ninth International Symposium on Structural Engineering for Young Experts*, Fuzhou & Xiamen, China.

Harries, K.A. (2008), "FRP components for bridge superstructures-US perspective", Fourth International Conference on FRP Composites in Civil Engineering, CICE2008, Zurich, Switzerland.

Hulatt, J., Hollaway, L. and Thorne, A. (2003), "Short term testing of hybrid T beam made of new prepeg material", *ASCE J. Compos. Construct.*, **7**(2), 135-144.

Khennane, A. (2009), "Manufacture and testing of a hybrid beam using a pultruded profile and high strength concrete", *Au. J. Struct. Eng.*, **10**(2), 145-155.

Lam, L. and Teng, J.G. (2003a), "Design-oriented stress-strain model for FRP-confined concrete", *Constr. Build. Mater.*, **17**, 471-489.

Lam, L. and Teng, J.G. (2003b), "Design-oriented stress-strain model for FRP-confined concrete in rectangular columns", *J. Reinf. Plast. Comp.*, **22**(13), 1149-1186.

Mansur, M.A., Chin, M.S. and Wee, T.H., (1999), "Stress-strain relationship of high-strength fiber concrete in compression", *J. Mater. Civil Eng.*, **11**(1), 21-29.

Mirmiran, A. and Shahawy, M. (1997), “Behavior of concrete columns confined by fiber composites”, *ASCE J. Struct. Eng.*, **123**(5), 583-590.

Neely, W.D., Cousins, T.E. and Lesko, J.J. (2004), “Evaluation of In-Service Performance of Tom’s Creek Bridge Fiber-Reinforced Polymer Superstructure”, *ASCE J. Perf. Const. Facil.*, **18**(3), 147-158.

Parsons, I.D., White, S., Therriault, D. and Bignell, J. (2002), “Manufacture and Testing of a Filament Wound Composite Bridge Superstructure”, *Final Report for Highway IDEA Project 63*, Transportation Research Board, Washington, D.C. 20001, http://www.nationalacademies.org/trb/idea

Pessiki, S., Harries, K.A., Kestner, J.T., Sause, R. and Ricles, J.M. (2001), “Axial behavior of reinforced concrete columns confined with FRP jackets”, *ASCE J. Compos. Construct.*, **5**(4), 237-245.

Richart, F.E., Brandtzaeg, A. and Brown, R.L. (1928), “A study of the failure of concrete under combined compressive stresses”, *In: University of Illinois Buletin*, **185**.

Richart, F.E., Brandtzaeg, A. and Brown, R.L. (1929), “The failure of plain and spirally reinforced concrete in compression”, In: *University of Illinois Bulletin*, **190**.

Samaan, M., Mirmiran, A. and Shahawy, M. (1998), “Model of concrete confined by fiber composites”, *ASCE J. Struct. Eng.*, **129**(9), 1025-1031.

Setunge, S., Attard, M.M. and Darvall, P.L. (1993), “Ultimate strength of confined very high-strength concretes”. *ACI Struct. J.*, **90**(6), 632-641.

Shehata, I.A.E.M., Carneiro, L.A.V. and Shehata, L.C.D. (2002), “Strength of short concrete columns confined with CFRP sheets”, *Mater. Struct.*, **35**, 50-58.

Teng, J.G., Huang, Y.L., Lam, L. and Ye, L.P. (2007), “Theoretical model for fiber reinforced polymer-confined concrete”, *ASCE J. Compos. Construct.*, **11**(2), 201-210.

Toutanji, H., Han, M., Gilbert, J. and Matthys, S. (2010), “Behavior of large-scale rectangular columns confined with FRP composites”. *ASCE J. Compos. Construct.*, **14**(1), 62-71.

van Erp, G., Cattell C. and Ayers S., (2005), “The Australian approach to composites in civil engineering”, *Reinf. Plast.*, **49**(6), 20-26.

Williams, B., Shehata, E. and Rizkalla, S.H. (2003), “Filament-wound glass fiber reinforced polymer bridge deck modules”, *ASCE J.Compos. Construct.*, **7**(3), 266-273

Walraven, J.C. (1981), “Fundamental analysis of aggregate interlock”, *ASCE J. Struct. Eng.*, **107**(11), 2245-2270.

Xiao, Y. and Wu, H. (2003), “Compressive behavior of concrete confined by various types of FRP composite jackets”, *J. Reinf. Plast. Comp.*, **22**(3), 1187-1201.

Yankelevsky, D.Z. and Leibowitz, O. (1999), “Punching shear in concrete slabs”, *Int. J. Mech. Sci.*, **41**, 1-15.

Zhao, L., Burgueňo, R., Rovere, H.L., Seible, F. and Karbhari, V. (2000), “Preliminary Evaluation of the Hybrid Tube Bridge System”, Final Test Report Submitted to California Department of Transportation under Contract No. 59AO032, California.

CC